Photodegradation of polylactic acid: Characterisation of glassy and melt behaviour as a function of molecular weight

Ábris Dávid Virág [a], Csenge Tóth [a], Kolos Molnár [a,b,*]

[a] Department of Polymer Engineering, Faculty of Mechanical Engineering, Budapest University of Technology and Economics, Műegyetem rkp. 3. H-1111 Budapest, Hungary
[b] ELKH–BME Research Group for Composite Science and Technology, Műegyetem rkp. 3., H-1111 Budapest, Hungary

ARTICLE INFO

ABSTRACT

During the COVID-19 pandemic, UV-C germicidal lamps became widely available, even for household applications. However, their long-term degradation effects on the mechanical and rheological properties of polylactic acid (PLA) are still not well established. The relationship between degradation and its effects on the molecular structure and macroscale properties are hardly known. In this study, we investigated the effects of long-term exposure to UV-C irradiation on the properties of PLA and interpreted the results at the molecular scale. We performed gel permeation chromatography, Fourier-transform infrared spectroscopy and UV–Vis spectroscopy to analyse changes in chemical structure induced by the UV-irradiation. Then, we carried out thermal, rheological and tensile tests to investigate mechanical and melting properties, and we investigated the applicability of these test results to estimate molecular weight loss. We have created a 3D irradiation map that can facilitate the design of disinfection devices. Based on our results, we propose a maximum number of sterilisation cycles (13 cycles) for the tested PLA films that do not result in significant changes in tensile strength and modulus.

1. Introduction

In the pursuit of sustainability, bio-based polymers are also gaining ground in medical applications, particularly as bioresorbable implants or packaging materials for medical devices and disposables [1]. One of the most popular biobased materials is polylactic acid (PLA). PLA has a very wide range of applications, from surgical sutures [2] and thermo-regulating textiles [3] to state-of-the-art implants [4] and controlled-release packaging materials [5]. PLA is a biodegradable polyester, therefore, it is typically sensitive to environmental effects and prone to various types of degradation, such as bio-, hydrolytic and photodegradation.

The degradation is a complex process influenced by a variety of factors such as humidity, temperature, pH, isomer ratio etc. [6]. Therefore, the degradation mechanism also differs in different circumstances, but all involve main and/or side chain scission. Kopinke et al. [7] showed that the thermal decomposition of PLA is based on intramolecular transesterification. Elsawy et al. [8] found that in the case of hydrolytic degradation, the ester groups break down from the main chain and acid groups are created, which will accelerate the process due

to the decrease in pH and the number of H+ ions. In the case of photodegradation, Ikada [9] found that UV-C light indicates mostly Norrish II-type degradation mechanisms in PLA, which means that the main chain absorbs the photon breaking the C—O bonds. Olewnik-Kruszkowska et al. [10] found a different degradation mechanism based on the presence of acetic anhydride. This was also in accordance with the mechanism proposed by Therias et al. [11].

As a consequence of its sensitivity, PLA can be decomposed in soil [12], in industrial compost [13], and in water under certain circumstances [14], but it is also sensitive to UV radiation [15]. Sterilisability is a prerequisite for medical application, and most sterilisation procedures (high-energy irradiation, steam and heat) involve the material undergoing various chemical processes, which also affect its material properties and lead to degradation [16]. The sterilising effect of ultraviolet lamps emitting ultraviolet C (UV-C) irradiation became widely applied with the outbreak of the COVID-19 pandemic [17]. Recent studies have demonstrated that 222 nm (far-UV) UV-C light is harmless to the human skin or eye [18]. However, it is less effective against bacteria and viruses compared to 254 nm UV light [19]. 254 nm UV light can be used to disinfect air [20], liquids [21] or surfaces [22].

* Corresponding author at: Department of Polymer Engineering, Faculty of Mechanical Engineering, Budapest University of Technology and Economics, Műegyetem rkp. 3, H-1111 Budapest, Hungary.
E-mail addresses: viraga@pt.bme.hu (Á.D. Virág), tothcs@pt.bme.hu (C. Tóth), molnar@pt.bme.hu (K. Molnár).

Today, the most widely used sterilisation method is the ethylene oxide-based method, but its use is expected to decline due to the toxicity and flammability of ethylene oxide [23]. Therefore, it is important to understand the impact of alternative sterilisation processes. UV-C irradiation has the potential to fill this gap, however, its effects on the molecular structure of PLA is not fully explored. Predicting changes in material structure caused by degradation is of high importance for usability. Our aim is to identify parameters based on widely available, relatively easy to perform measurements that can be used to indicate the degree of molecular weight loss.

We subjected PLA films to different doses of UV-C irradiation. Based on the experimental data, we apply models to predict molecular weight loss, then, we establish relationships between the molecular weight and the material properties. We reveal the effects of degradation which greatly assist the design from processing to reuse. We measured the irradiance of the light source and calculated the dose levels, so these results can be interpreted for any known dose from any 254 nm UV-C source. This means that material property changes can be estimated after any number of sterilizations. Lastly, we propose a limit of repeated sterilisation, until which the PLA film still fulfils its function, and it is safe to use.

2. Materials and methods

2.1. Material and film sample preparation

The polylactic acid (PLA) used in this study was an extrusion grade PLA, namely Ingeo 4032D (supplied by NatureWorks LLC, Plymouth, MN, USA), with a density of 1.24 g/cm^3 and a D-lactide content of only 1.4–2 % [24]. The number- (M_n) and weight-average (M_w) molecular weight of the neat material are 124.0 and 228.9 kg/mol, respectively (measured by gel permeation chromatography).

Before processing, the material was dried in a Faithful WGLL-125 BE (Faithful Instrument (Hebei) Co., Ltd., Huanghua, China) hot air oven at 80 °C for 4 h. The optically transparent PLA film was produced with a Labtech Scientific 25-30C single-screw extruder (Labtech Engineering, Thailand) and an LCR300 flat film line (Labtech Engineering, Samutprakarn, Thailand). The extruder included a general-purpose three-zone screw with a diameter of 25 mm and a length/diameter ratio (L/D) of 30. We used a 300 mm wide coat-hanger flat film die with a 0.6 mm gap size to produce the films. The temperature profile from the hopper to the die was 200 °C–200 °C–210 °C–210 °C, while the temperature of the die was set to 220 °C. The screw speed was 35 rpm. The temperature and peripheral speed of the tempered, polished take-up cylinder were 60 °C and 1 m/min, respectively. The circumferential speed of the traction roller was 1.8 m/min, hence the draw ratio was 1.8. After extrusion, the samples were left to rest for one week in sealed packages containing grains of silica gel to exclude the effect of humidity and to ensure that physical ageing occurred. The thickness of the films produced was 170 ± 20 μm.

2.2. Photodegradation treatment and related conditions

We custom-built a degradation chamber (Fig. 1/a, b, c) equipped with two TUV30W Longlife SVL (Philips, Amsterdam, Netherlands) mercury-vapour tube lamps. The UV tubes have a diameter of 28 mm and a length of 0.9 m, emitting 254 nm wavelength radiation with a narrow spectral power distribution. To measure the irradiance of the mercury lamp, we used an RM-12 type radiometer with a UVBB radiometric sensor (UV Messtechnik Opsytec Dr. Gröbel GmbH, Ettlingen, Germany) which was responsive in the 230–400 nm spectral range. Fig. 1/d shows the measurement spots. We measured the irradiance at 6 different points along the x-axis (which coincides with the centre line of the tube) to determine the irradiance along the length of the tube. Then, we determined the irradiance along the z distance and the angle of incidence (φ). We measured the irradiance at 10 different points between 0 and 257 mm in the z-direction and at 7 different points between 0 and 150 mm in the y-direction. The angle of incidence was calculated
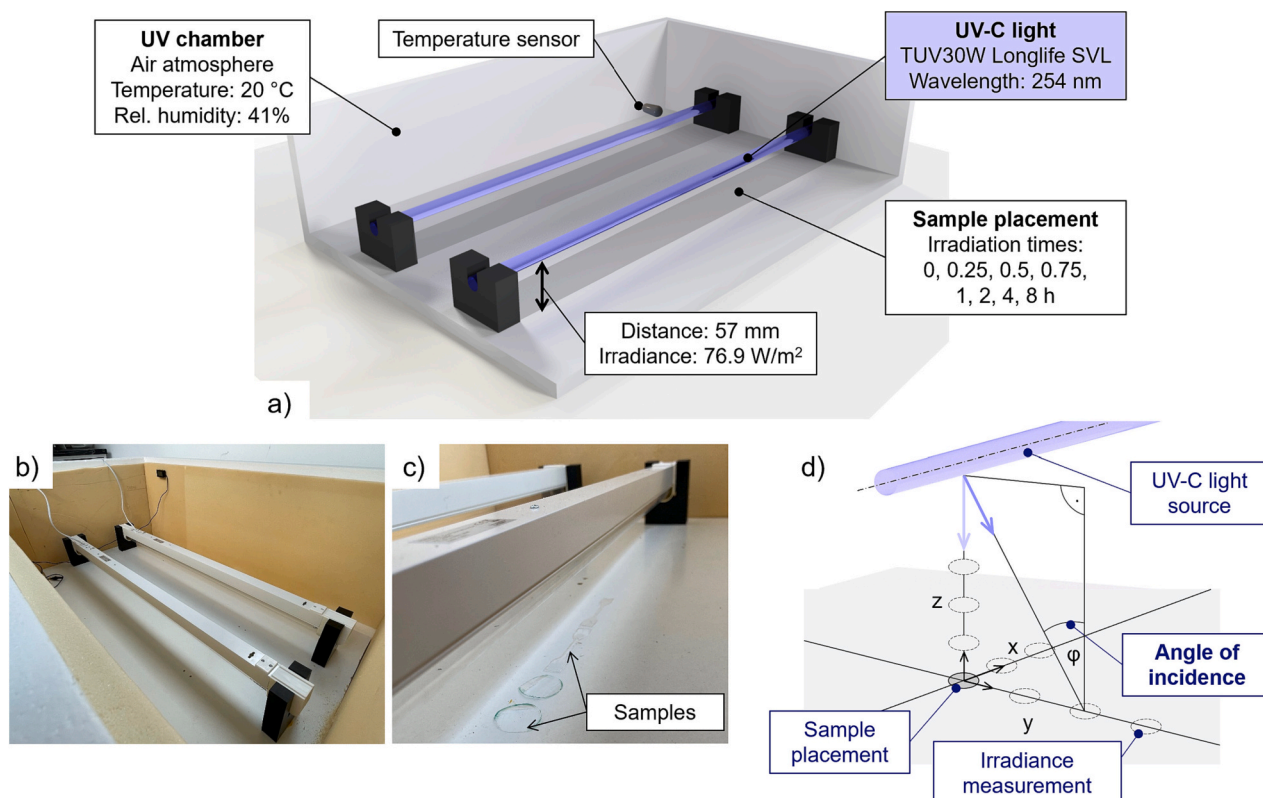

Fig. 1. Schematic of the UV chamber (a), the actual setup (b), the disk- and dumbbell-shape irradiated samples (c), the spots used for irradiance measurement (d).

as $\varphi=\arctan(y/z)$ from the right-angled triangle in Fig. 1/d. The two light sources are placed at such a distance that only one light source has a significant degradation effect on the test specimen placed under the tube (400 mm). We irradiated the PLA films in an air atmosphere for various exposure times at 20 °C ambient temperature and 41 % relative humidity. The following irradiation times were used: 0, 0.25, 0.5, 0.75, 1, 2, 4 and 8 h. We placed the samples under the UV-C tube at $\varphi=0°$ and z = 57 mm. We calculated the UV dose (also known as fluence) (kJ/m^2) as the product of irradiance (kW/m^2) and irradiation time (s).

2.3. Fourier-transform infrared spectroscopy (FTIR)

We performed Fourier Transform Infrared (FTIR) spectroscopy measurements on the surface of the samples using ATR-FTIR (Fourier-Transform Infrared Spectroscopy) apparatus (Bruker Tensor II, Bruker OpticsInc., Billerica, MA). Its wavelength range is from 4000 to 400 cm^{-1}. Sixteen scans were performed and averaged on each sample.

2.4. UV–visible spectroscopy (UV–vis)

Light transmittance of the films was measured with an Agilent 8453 UV–Vis spectrometer (Agilent Technologies Inc., Santa Clara, CA, USA) in the range of 200–600 nm wavelength. The undegraded PLA and the samples irradiated for 1 h, 2 h and 4 h were investigated.

2.5. Differential scanning calorimetry (DSC)

Modulated differential scanning calorimetry (MDSC) tests were performed in accordance with the ISO 19935-2:2020 standard on 8–10 mg film samples in an inert (nitrogen) atmosphere at a purge flow rate of 50 ml/min with a TA Q2000 device (TA Instruments, New Castle, DE, USA). The modulation amplitude was 0.8 °C, and its oscillation period was 60 s. We applied a heat/cool/heat cycle between 0 and 200 °C with a heating/cooling rate of 5 °C/min. We performed the first heating and cooling cycle to eliminate the thermal history of the samples. The glass transition temperature (T_g) was determined as the maximum of the temperature derivative of the reversible heat capacity signal from the 2nd heating cycle. Melt temperature (T_m) was determined as the peak of the enthalpy change associated with crystal melting. We performed 3 tests in each case.

2.6. Tensile testing

We carried out tensile testing in accordance with the ISO 527-2:2012 standard. We cut tensile specimens from the extruded films parallel to the extrusion (processing) direction using a manual punching machine. The shape of the specimens was in accordance with the type 5A dumbbell specimen of the ISO 527-2:2012 standard and it had a total length of 75 mm. Uniaxial tensile tests were carried out at 25 °C with a Z005 (Zwick Gmbh., Ulm, Germany) universal tensile tester using 200 N rated Zwick 8131 type screw grips. In every case, we performed 9 parallel displacement-controlled tests with a 50 mm gripping distance and a 2 mm/min crosshead speed. The sample irradiated for 8 h was degraded to the extent that it was fractured during gripping and could not be tested. The force was measured with a high-precision Zwick 5 kN load cell with a resolution of 0.01 N. Strain was calculated as the ratio of crosshead displacement and gripping distance. We determined the tensile modulus as a chord slope between 0.05 % and 0.15 % strains. We chose 0.15 % (instead of the standard 0.25 %) because the elongation at break of highly degraded samples was <0.25 %. We calculated tensile toughness (W) in J/cm^3 by integrating the area under the stress–strain (σ-ε) curve, where the units of stress and elongation are MPa and 1, respectively.

2.7. Rheological characterisation

The rheological properties of the neat and degraded PLA samples were investigated with an MCR-301 (Anton-Paar, Graz, Austria) rotational rheometer in accordance with the ISO 6721-6:2019 standard, using a parallel-plate geometry setup with an upper plate diameter of 25 mm and a gap size of 1 mm. Measurements were carried out in oscillation mode at 180 °C. Discs of 25 mm diameter were cut from the extruded sheets. Six discs were stacked together to fit the 1 mm gap. After loading the samples, we applied a five-minute retention time to reach thermal equilibrium and allow relaxation processes. To determine the linear viscoelastic region (LVER), we performed strain sweep experiments between 0.1 % to 10 % oscillation strain at an angular frequency of $\omega = 628$ rad/s. Then, frequency sweeps with an oscillation strain of 5 % were conducted in the frequency range of 0.0628 to 628 rad/s in every case.

2.8. Measuring the molecular mass

We performed gel permeation chromatography/size exclusion chromatography (GPC/SEC) analyses to investigate the changes in molecular weight and molecular weight distribution due to UV-C irradiation. A VE 1122 solvent delivery system (Viscotek, Malvern Panalytical, Worcestershire, UK) was used with a Shodex SE 61 refractive index detector (Showa Denko, Tokyo, Japan). Analysis was performed using a volume of 10 μl chloroform solution with 0.5 % m/V concentration at 35 °C and at a flow rate of 1 ml/min. We used two Mixed-C Styragel columns with a mixed bed (Agilent Technologies Inc., Santa Clara, CA, USA), capable of a linear range of M_w = 200–2,000,000 g/mol. To generate the calibration curve, we used EasiCal Pre-prepared Calibration Kits polystyrene standards (Agilent Technologies Inc., Santa Clara, CA, USA) with a narrow molecular weight distribution [25]. We calculated the M_n and M_w values of the samples irradiated for 0, 0.25, 0.5, 1, 2 and 8 h.

2.9. Statistical analysis

We used the Minitab 21.1.0 statistical software (Minitab LLC, State College, PA, USA) for statistical analysis and performed the model fittings in Matlab R2022a software (Mathworks, Natick, MA, USA). All data were expressed as means ± standard deviation. We assumed normality and equal variance and used the Ryan-Joiner normality test and Levene's test for equality of variances to examine our assumptions. In the case of melt temperature and tensile strength, these assumptions were not violated, so we used one-way analysis of variance (ANOVA) with a *post-hoc* Tukey HSD (Honestly Significant Difference) test to examine the differences among different groups. For tensile modulus, the variances were unequal, hence we used Welch's ANOVA with the Games-Howell *post-hoc* test. Our null hypothesis in all cases tested was that all means are equal. For curve fitting, we used the least square method. The coefficient of determination (R^2) values reported in the study are always the adjusted R^2 values. For all analyses, a significance level of $\alpha = 0.05$ was used.

3. Results and discussion

3.1. Dependence of irradiance on distance and angle of incidence

The distance-dependent irradiance of the UV light source used in this study is shown in Fig. 2. The irradiance along the tube can be considered uniform since the deviation of the measured points is small (in most cases smaller than the size of the marker used). The irradiance decreases as the distance from the tube increases. The decrease in irradiance can be approximated very accurately ($R^2 > 0.998$) with the following empirical model (Eq.1):
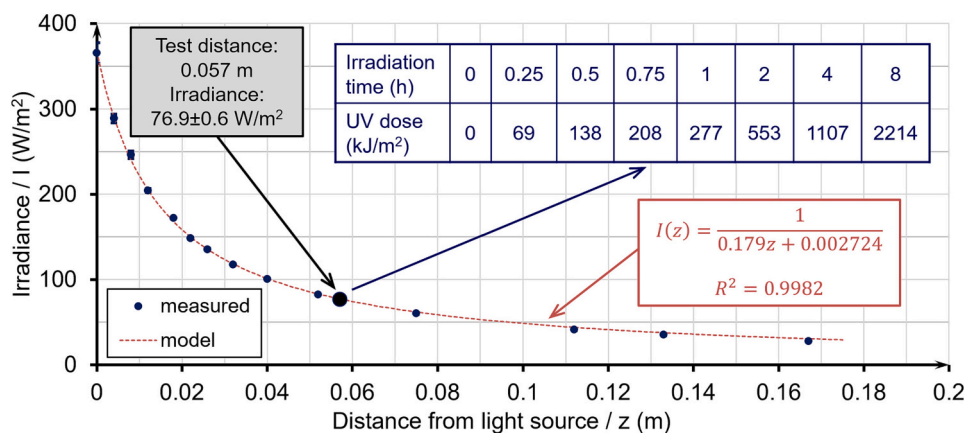
Fig. 2. Irradiance as a function of distance from the light source (measured data and model). In most cases, the standard deviation of the measured points is smaller than the size of the marker used.

$$I = \frac{1}{k \cdot z + b} \qquad (1)$$

where I (W/m^2) is irradiance, k (m/W) is the rate of decrease, z (m) is the distance from the light source and b (m^2/W) is the inverse of the initial irradiance (measured at $z = 0$ m). Hence the inverse of irradiance $(1/I)$ is proportional to the distance from the light source (z). The fitted model parameters are the following: $k = 0.179$ m/W and $b = 2.724 \cdot 10^{(-3)}$ m^2/W. The UV dose calculations can be used to determine the irradiation times and distance necessary for proper disinfection. In case of SARS-CoV-2 viruses, the lethal dose for 99.999 % viral inactivation was 1.09 kJ/m^2 [26]. Mills et al. [27] achieved the complete decontamination of N95 respirators infected with the H1N1 influenza virus using a UV dose of 10 kJ/m^2, and that value is considered the minimal required dose for decontamination of all surfaces to ensure the safety of healthcare workers [28]. Based on these findings, under the sterilisation conditions used in our study, adequate disinfection is achieved in 0.036 h (131 s). Also, long-term irradiation experiments can be interpreted as repeated disinfections, which enables to determine the extent to which the properties of a given product change over repeated re-disinfection, and thus provide a limit to its reusability.

Irradiance also depends on the angle of incidence. Fig. 3 shows the irradiance map, i.e., the irradiance as a function of the distance from the light source (z) and the angle of incidence (φ). The irradiance decreases as the distance and/or the angle increases. The results show that at the
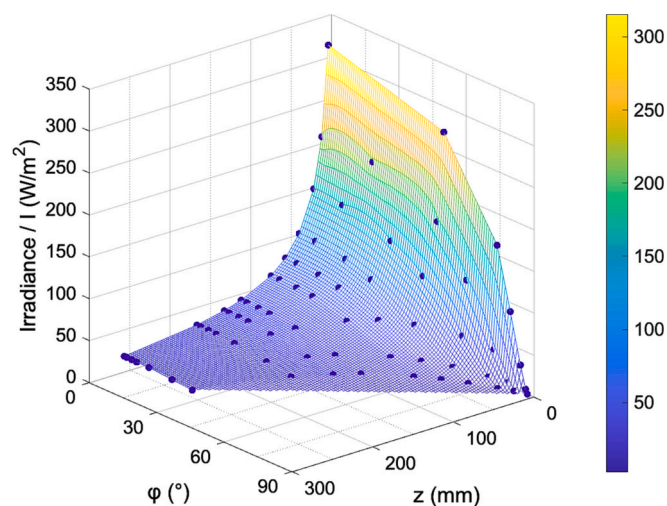
sample placement distance, the difference between the irradiance values along the y-axis (Fig. 1/d) is less than 3 % even for the widest sample (25 mm). This means that the whole surface of the samples is exposed to a uniform UV dose, therefore the sampling location does not affect the further results. The UV dose varies according to the relative spatial position (z, φ) of the lamp and the sample, but the irradiance map allows these dose values to be determined for specific irradiation times. The dose is a quantity that can be interpreted in general terms, including the parameters of the radiation source, the relative position of the radiation source and the sample, and the exposure time. Therefore, the irradiance map facilitates the design of disinfection devices and the development of disinfection techniques.

3.2. Changes in molecular weight (GPC results)

Besides measuring the molecular mass of neat samples, we quantified the irradiation-induced degradation using GPC. Fig. 4/a shows the molecular weight distribution of the PLA samples. With increasing irradiation time, the distribution curves shifted towards the lower molecular weights, but the shape and characteristics of the monomodal distribution curves remained similar for up to 2 h (homogeneous degradation). Dispersity (Đ) (also known as polydispersity index) increased by 2 % up to two hours of irradiation and then increased by 25 % at 8 h. Similar trends in polydispersity were reported by Yasuda et al. [29] in the case of the UV-C irradiation of PLA samples.

Table 1 and Fig. 4/b show the absolute (M_n and M_w) and normalised ($M_{n,norm}$ and $M_{w,norm}$) number- and weight average molecular weight as a function of irradiation time. We carried out normalisation by dividing each data series by the maximum value of the data series. Irradiation reduced the number- and weight-average molecular weight by 48 % after half an hour, and by 79 % in 2 h, compared to the undegraded, virgin PLA. The normalised average molecular weights are close, therefore the thermal, rheological and tensile behaviour characteristic of M_n is very similar to that of M_w, and vice versa.

The mechanism of degradation can be determined from the relationship between the inverse of the number-average molecular weight $(1/M_n)$ and irradiation time. Linear regression fitted the data well ($R^2 > 0.995$), thus in accordance with the paper of Gleadall et al. [30], we can conclude that this photolysis is pure non-catalytic random scission (Fig. 4/c). The degradation mechanism is a second-order reaction, which can be described with Eq. 2:

$$\frac{1}{M_n} = k \cdot t + \frac{1}{M_{n,inital}} \qquad (2)$$

where k is the rate constant of the photolysis process. The rate constants are 0.0186 and 0.0072 mol/(kg·h) for number- and weight-average

Fig. 3. Irradiance map: the irradiance as a function of distance from the light source (z) and the angle of incidence (φ).
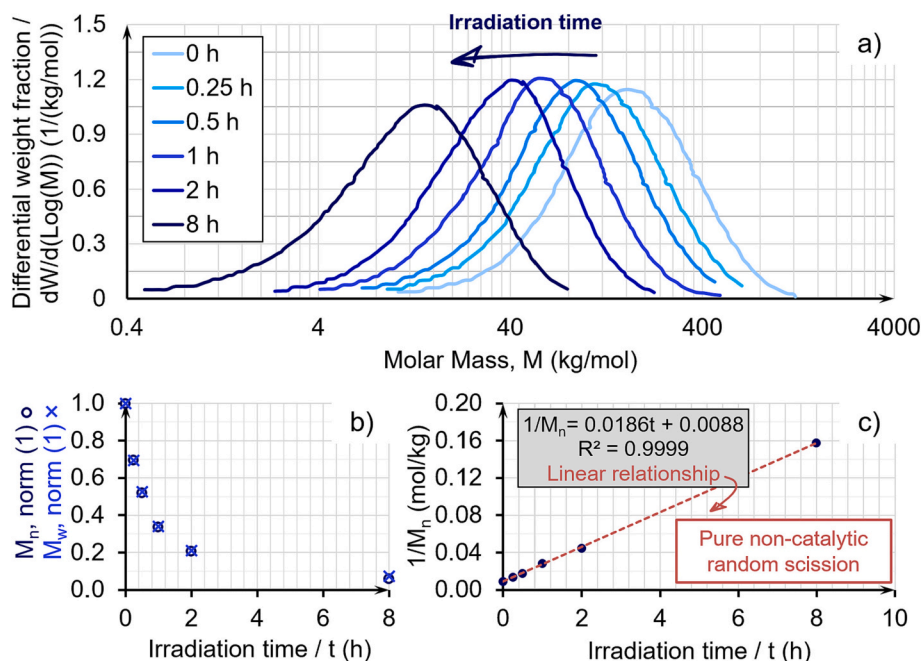
Fig. 4. Changes in molecular weight as a function of irradiation time: molecular weight distribution of the irradiated PLA samples (a), normalised number- and weight-average molecular weight (b), and the connection between the inverse of number-average molecular weight and irradiation time (c).

Table 1
GPC results of PLA samples irradiated with UV-C light for different times.

Irradiation time (h)	M_n (kg/mol)	M_w (kg/mol)	Đ (1)	$M_{n, norm}$ (1)	$M_{w, norm}$ (1)
0	107.20	208.0	1.94	1.00	1.00
0.25	74.49	144.6	1.94	0.69	0.70
0.5	55.74	109.6	1.97	0.52	0.53
0.75	43.96*	87.72*	2.00*	0.41*	0.42*
1	35.84	70.90	1.98	0.33	0.34
2	22.28	44.02	1.98	0.21	0.21
4	12.02*	28.74*	2.39*	0.11*	0.14*
8	6.34	15.81	2.50	0.06	0.08

* calculated from a linear regression curve.

molecular weights, respectively. The non-catalytic random scission of PLA subjected to UV-C light was also reported by Olewnik-Kruszkowska et al. [10], Santonja-Blasko et al. [31] and Yasuda et al. [29]. Since UV-C irradiation does not affect polydispersity, with the help of the molecular weight distribution of the neat polymer, average molecular weights and the distribution curves can be estimated up to 80 % degradation.

3.3. Changes in chemical structure (FTIR results)

We carried out FTIR spectroscopy on the reference and on the irradiated film surfaces to investigate the changes occurring at the molecular level. The FTIR spectra of the neat and degraded samples can be seen in Fig. 5/a. We assigned the peaks based on the literature [10,32,33]. At 3300 cm^{-1} a broad peak appeared, which was found to correspond to alcohol and carboxylic acid groups [11]. The band at 2999 cm^{-1} is assigned to the asymmetrical stretching vibrations, and the band at 1450 cm^{-1} indicates the asymmetrical deformation vibration of the CH$_3$ group. The increase of carboxylic acid groups and CH$_3$ can indicate the formation of acetic acid due to photodegradation. Therias et al. [11] also identified oxalic acid, carbonic acid and formic acid as possible end products. Based on the increase in -COOH groups, Zhang et al. [34] proposed a possible photodegradation mechanism shown in Fig. 5/b. This mechanism is also supported by the fact that similarly to the results of Zhang et al. [34] the band originally at 1749 cm^{-1} shifts to

1745 cm^{-1} after 4 h of degradation. The band at 1749 cm^{-1} is attributed to the stretching vibrations of the carbonyl group.

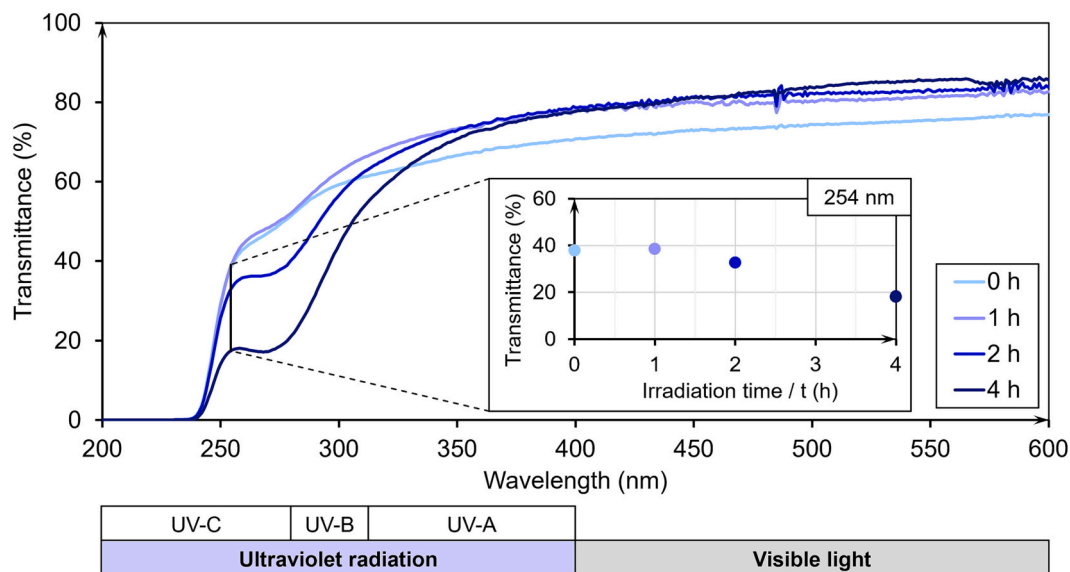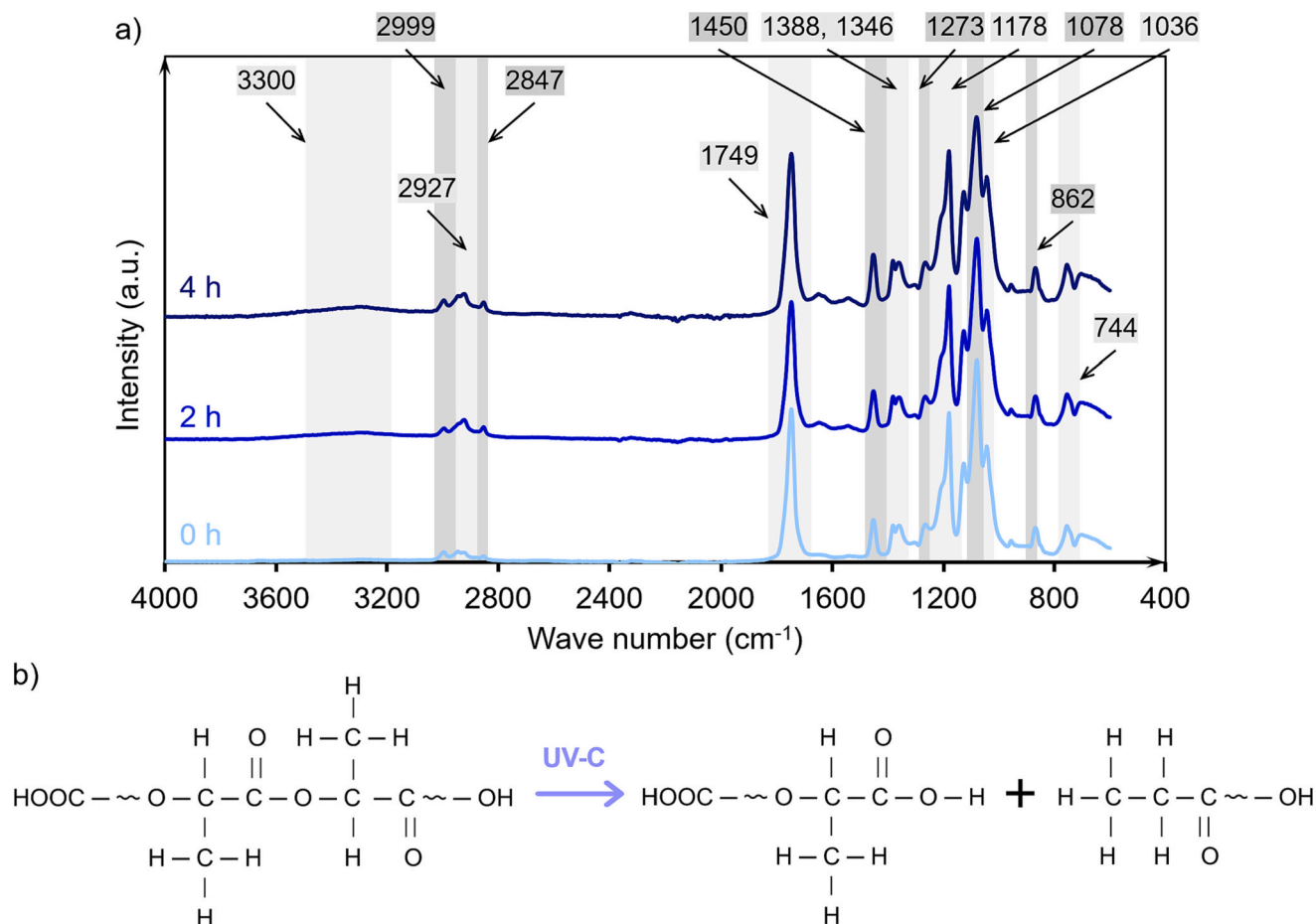### 3.4. Changes in transmittance (UV–vis results)

Fig. 6 shows the light transmittance as a function of wavelength in the UV- and visible light range. In the UV-C range, there is no change in transmittance up to 1 h, and then as degradation progresses, the transmittance decreases, therefore during degradation the UV-C shielding effect of the films increases. This can indicate an increase in the number of carboxyl groups, which have stronger absorbance [35]. This is also consistent with the FTIR results. In the visible light range, there is a slight increase in the transmittance with increasing degradation time. No discolouration or change in surface structure was observed.

3.5. Changes in transition temperatures (DSC results)

We carried out DSC tests to determine the first- and second-order transition temperatures, T_m and T_g respectively. Fig. 7 shows the second heating curves. Crystallisation enthalpy and cold crystallisation enthalpy were the same in each case, which means the samples were completely amorphous. For short irradiation times (up to 0.75 h), the transient temperatures showed a variation of only 1.3 °C, and for long-term degradation, the maximum variation was 16 °C (in the case of T_g).

Compared to the drastic changes in molecular weight (a decrease of 59 % and 94 % at 0.75 h and 8 h, respectively), the decrease in transition temperatures can be considered small, especially for short-term irradiation. Transition temperatures are associated with the energy required for molecular motion, which is strongly influenced by the number of secondary bonds [36]. The small variation in the transition temperatures for short irradiation times means that after irradiation, there was no significant remaining damage to the secondary bonds. Meanwhile, molecular weight decreased, which also supports that the dominant degradation mechanism is primary bond breakage.

Fig. 8/a and b shows T_g and T_m as a function of the number-average molecular weight, respectively. T_g values between 40 and 80 kg/mol are approximately equal, but the standard deviation of the results is much higher than the difference between the means. Below 40 kg/mol, T_g

Fig. 5. FTIR spectra of the neat and degraded samples (a) and possible photodegradation mechanism [34] (b).

Fig. 6. Changes in the UV–Vis spectra as a function of irradiation time.

starts to decrease. Fig. 8/b shows that there is a transition (number-average) molecular weight around $M_{trans} \approx 55.74$ kg/mol (0.5 h irradiation time), above which there is no significant change in the melting temperature ($p = 0.889$).

The dependence of T_g and T_m on M_n can be described with the Flory-Fox (Eq.3) [37], and the Flory empirical equations (Eq.4) [38], respectively:

$$T_g = T_g^\infty - \frac{K_1}{M_n} \tag{3}$$
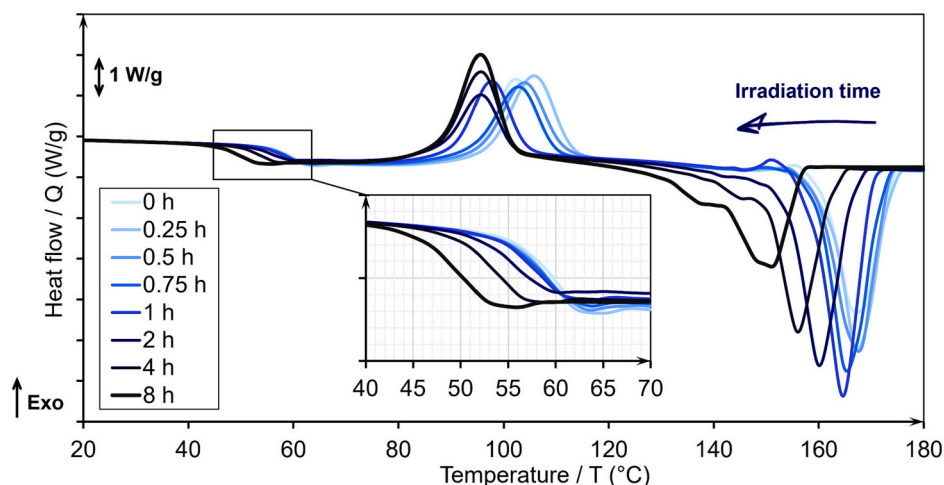
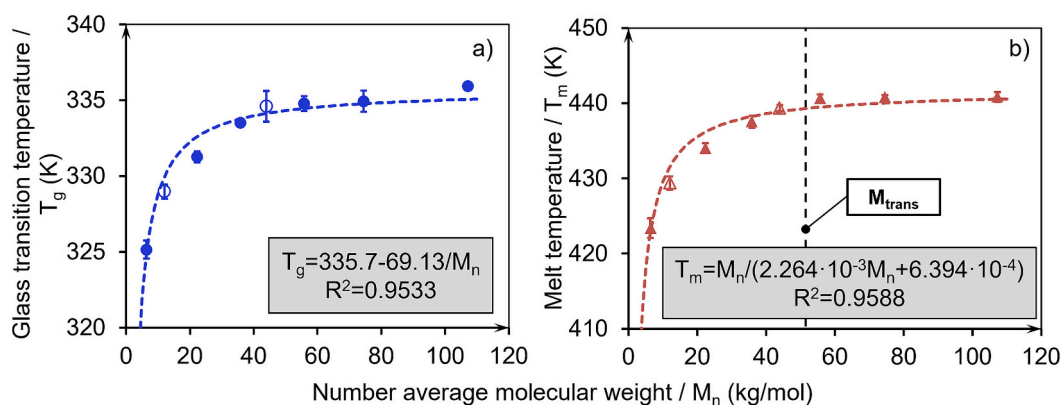**Fig. 7.** Second heating curves of PLA samples irradiated with UV-C light.

Fig. 8. Glass transition temperature (a) and melting temperature (b) as a function of the number-average molecular weight. The full circles are the properties associated with the measured molecular weights; the empty circles are the measured properties associated with the molecular weights estimated from linear regression. For the fitting, we used only the full circle data.
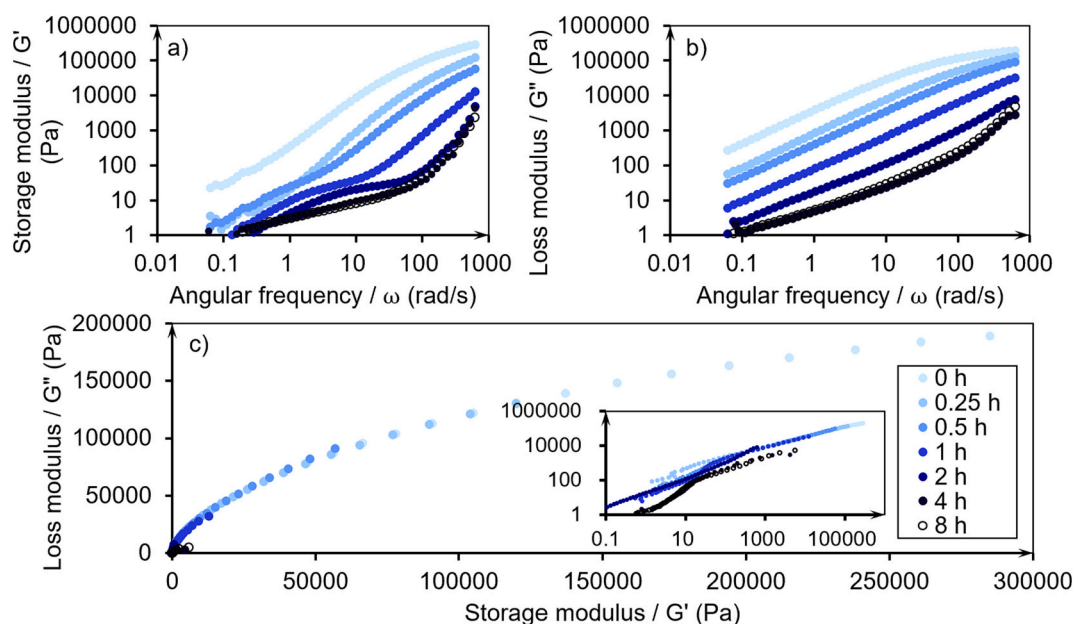

Fig. 9. Dynamic rheological properties of PLA samples irradiated with UV-C light for different times: a) Storage modulus, b) Loss modulus, c) Han plot.

$$\frac{1}{T_m} = \frac{1}{T_m^\infty} + \frac{2RM_0}{\Delta H_m M_n} \rightarrow T_m = \frac{M_n}{\frac{1}{T_m^\infty}M_n + \frac{2RM_0}{\Delta H_m}} \qquad (4)$$

where K_1 (K·kg/mol) is the Flory-Fox constant (fitted parameter), which is related to the free volume present in the polymer, T_g^∞ (K) and T_m^∞ (K) are the limiting glass transition and melting temperature for very high molecular weight (both are fitted parameters), $R = 8.314$ J/(mol·K) is the universal gas constant, $M_0 = 0.07206$ kg/mol is the molecular weight of the repeat unit of PLA and ΔH_m (J/mol) is melting enthalpy (a fitted parameter). According to the fitted equations, the fitted parameters are the following: $T_g^\infty = 335.7$ K, $K = 69.13$ K·kg/mol, $T_m^\infty = 441.7$ K, $\Delta H_m = 1874$ J/mol. There are other similar, empirical equations that relate transition temperatures to molecular weight like the Fox and Loshaek equation [39]. These models can be used for prediction at lower molecular weights (higher degradation). As we mentioned previously, there is no significant change in T_m until the average molecular weight is reduced by half. Also, for PLAs with a higher molecular weight than 100 kg/mol, T_g is approximately constant for a given ʟ-lactide percentage [40]. Therefore, the transition temperatures are not a good indicator for estimating the UV-C irradiation-induced degradation of PLA.

3.6. Changes in the rheological properties (dynamic test results)

We carried out tests with a rotational rheometer to investigate the changes in dynamic rheological properties. Figs. 9/a and b show the storage and loss modulus, respectively, while Fig. 9/c shows the dependence of the loss modulus on the storage modulus (generally referred to as the Han plot). Moduli decreased gradually with increasing irradiation time. GPC measurements proved that UV-C irradiation induces chain scission. Shorter chains are more mobile as fewer secondary bonds restrict them (compared to longer chains), hence they have lower resistance to shear. The Han plot shows that the curves are identical in shape, but their length decreases as irradiation time increases. The exceptions to this are the 4- and 8-h tests, which do not fit the trend and have minimal differences between them.

Fig. 10/a shows the complex viscosity curves as a function of irradiation times. (According to the Cox-Merz rule, complex viscosity as a function of frequency can be converted to steady-state viscosity as a function of shear rate [41].) Complex viscosity at a given frequency (1 rad/s) decreased by 78 %, 98 %, and 99.9 % after 0.25 h, 1 h, and 8 h of irradiation, respectively. As molecular weight decreases, the frequency-dependent behaviour of the polymer melt also changes (Fig. 11). The undegraded sample showed Newtonian behaviour at lower shear rates, then shear thinning above 100 rad/s. This is the expected behaviour of a polymer melt. Shear causes the chains to align in the direction of flow and reduces the physical contact between them, allowing greater mobility and thus reducing viscosity. As the chains are broken by degradation, relaxation times are shortened, and molecules can respond faster to shear. This results in the gradual disappearance of the shear thinning phase, and at a certain point (at 1-h irradiation) the curve

becomes Newtonian over the whole frequency range tested. Below $M_n = 36$ kg/mol (for irradiations longer than 1 h) we can see that the frequency-dependent behaviour of complex viscosity further changes. Increasing frequency induces shear thinning up until 100 rad/s. Then, shear thickening can be observed. This suggests possible branching [42] caused by the high temperature. The possibility of branching is also supported by the van Gurp-Palmen plot (Fig. 7/b). The viscoelastic behaviour of polymers can be described along the y-axis, and at the phase angle of 90°, the presence of a plateau means an ideally viscous fluid. As molecular weight decreases, the plot shows a decrease towards the elastic region instead of a plateau. Marek and Verney [43] found similar results in their study of the time-dependent rheological behaviour of PLA under the combined effects of high temperature and UV radiation using an excitation frequency of 1 rad/s.

The rheological data can be used to estimate changes in average molecular weight. There is a strong correlation between the zero-shear viscosity and the weight average molecular weight of linear amorphous polymers, as described by Fox and Loshaek (Eq.5) [44]:

$$\eta_0 = K_2 \cdot M_w^\alpha \qquad (5)$$

where K_2 (Pas/(mol·kg)$^\alpha$) is a material- and temperature-dependent constant and α is a power-law exponent. We approximated zero shear viscosity ($\eta_{0, avg}$) as the average of the viscosities between 0.1 and 10 rad/s. However, in addition to viscosity (often used in the literature), other rheological properties may also be suitable for estimation. The loss modulus shows quasi-linearity on a log-log scale between 0.1 and 100 rad/s, therefore it can be a good indicator. The Han curves also change according to a trend, up to 4 h of irradiation. We also calculated the average loss moduli (G''_{avg}) between 0.1 and 10 rad/s, and the areas under the Han curves (A_{Han}). Table 2 shows the results.

Eq. 5 can be linearised by taking the logarithm of both sides. We assumed the same relationship between G''_{avg} and M_w, and for the A_{Han} as well, and fitted linear functions according to Eq. 6.

$$\text{Log}(\eta_0) = \text{Log}(K_2) + \alpha \cdot \text{Log}(M_w) \qquad (6)$$

Fig. 12 shows the results of the fitting. Up to 80 % degradation, these parameters characterise the degree of degradation and show a strong correlation with the decrease of M_w. For viscosity, α is close to 3.4 which is in agreement with the literature [45]. The measurement results after 8 h irradiation were not taken into account in the fitting, because it clearly does not fit the trend. This is probably because at this level of degradation, the frequency sweep test provides a questionable estimation for zero shear viscosity, and the structure of the material changed, as supported by the van Gurp-Palmen (Fig. 10/a) and Han plots (Fig. 10/b). A further possible explanation is that M_w after 8 h (16 kg/mol) is smaller than the critical molecular weight (M_c) itself. However, M_c is around 9 kg/mol in the literature for a PLA containing 2 % ᴅ-lactide [46,47]. We conclude that the decrease in molecular weight due to irradiation between 0 and 2 h can be estimated well with all the three material properties studied since the coefficients of determination were
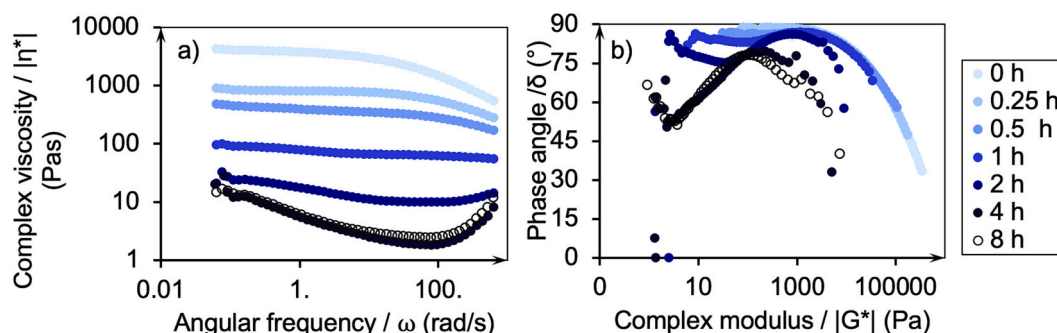

Fig. 10. Complex viscosity curves (a) and van Gurp-Palmen plot (b) of PLA samples irradiated with UV-C light for different times.
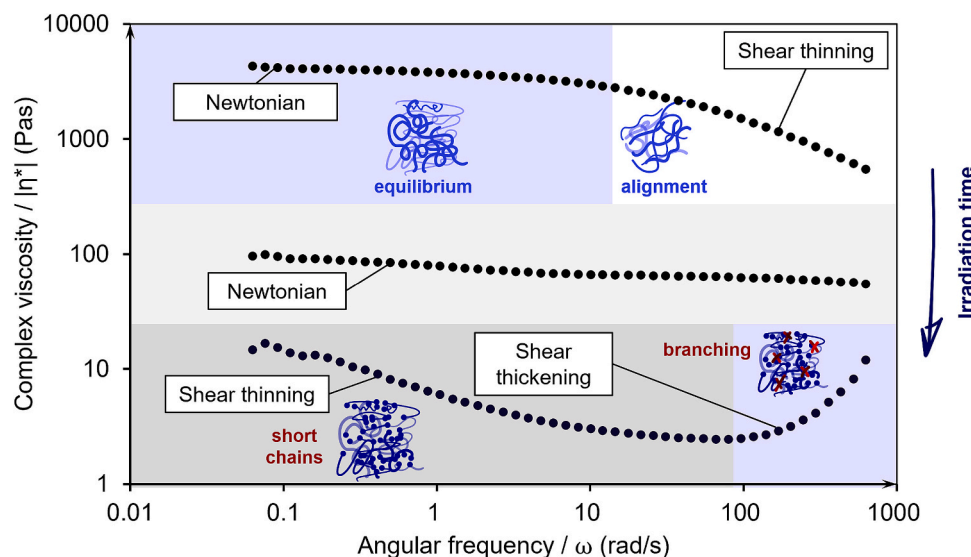
Fig. 11. Changes in the shape of the viscosity curve due to irradiation.

Table 2
Calculated averages of dynamic rheological properties.

Irradiation time (h)	$\eta_{0, avg}$ (Pas)	G″$_{avg}$ (Pa)	A ((kPa)^2)
0	3804	5228	37,200
0.25	823.1	1229	10,080
0.5	409.8	576.1	3176
1	81.80	110.3	266.7
2	19.32	21.55	29.01
4	8.460	5.520	9.990
8	8.340	6.160	19.17

close to 1 in all cases ($R^2 > 0.99$).

3.7. Deterioration of the tensile properties (tensile test results)

We carried out tensile tests to analyse the changes in mechanical properties. We first describe the changes in tensile properties, then we present models to predict molecular weight loss from the tensile data. Finally, we provide a molecular-based explanation for the difference in failure modes as a function of molecular weight.

3.7.1. Ductile-brittle transition

Fig. 13 shows the tensile curves obtained after different irradiation times. As irradiation time increases, the shape of the curve remains unchanged, only elongation at break decreases. This phenomenon can also be observed in the study of Szatkowski et al. [48] and Pinpathomrat

et al. [49], but since their research focused on the effect of carbon reinforcement, they did not address it. Fig. 13 also shows that there is a transitional (number average) molecular weight value around $M_{trans} = 55.74$ kg/mol at 0.5 h irradiation, above which the material is ductile and below which it is brittle.

Fig. 14/a shows tensile strength and elongation at break as a function of M_n, and Fig. 14/b shows the tensile toughness and Young's modulus. Elongation at break and tensile toughness decrease with increasing irradiation time from the beginning. Above M_{trans} the tensile strength of the degraded samples showed no statistically significant difference compared to the neat sample (see Table A.1). After 0.5 h of UV-C treatment (below M_{trans}), tensile strength decreased. The moduli of the degraded samples are statistically identical to the modulus of the neat polymer (see Table A.2). As the stiffness of glassy polymers depends on secondary bonds, the constancy of modulus is expected [50]. The constancy of yield stress and modulus, and the decrease of elongation at break were also observed by Pabiot and Verdu [51] during tensile testing of photochemically aged polyethylene, polypropylene and poly-vinyl-chloride. Fayolle et al. [52] observed similar phenomena when studying the thermal oxidation of polypropylene films. However, these phenomena have not yet been reported for polylactic acid.

3.7.2. Estimation of molecular weight loss based on tensile properties

Molecular weight can also be estimated with the use of tensile properties. The Flory equation (Eq. 7) [53] describes the relationship between the number-average molecular weight and tensile strength:
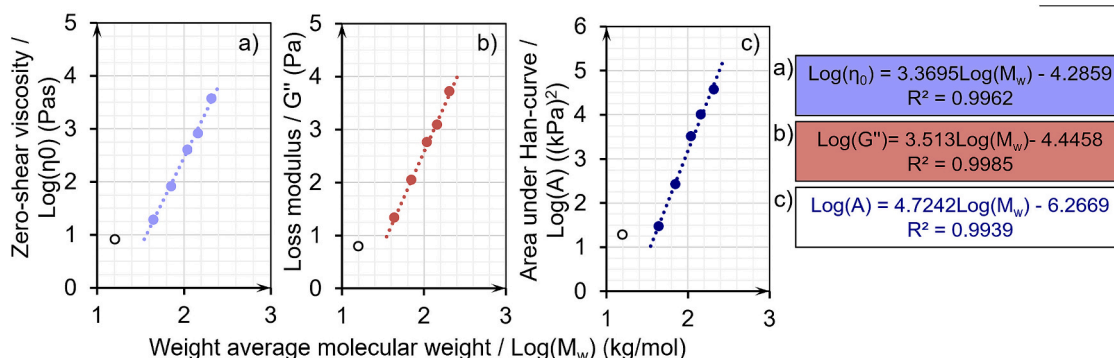

Fig. 12. Connection between weight average molecular weight and dynamic rheological properties of PLA samples irradiated with UV-C light for different times: a) Zero-shear viscosity, b) Loss modulus, c) Area under the Han curve.
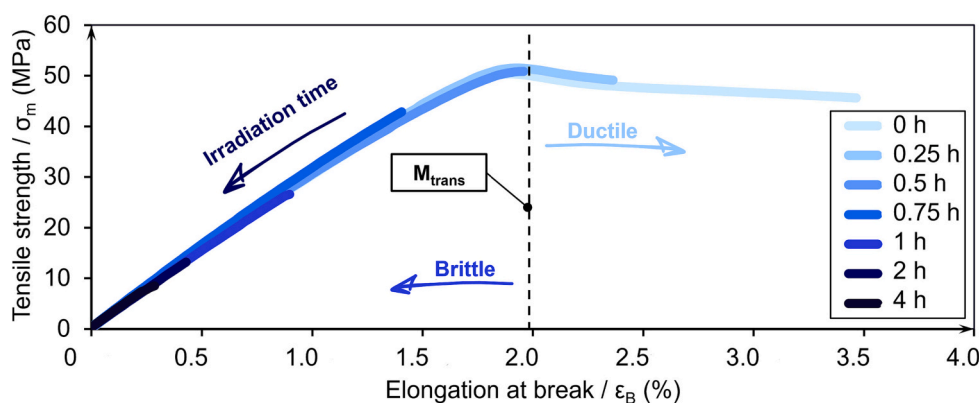
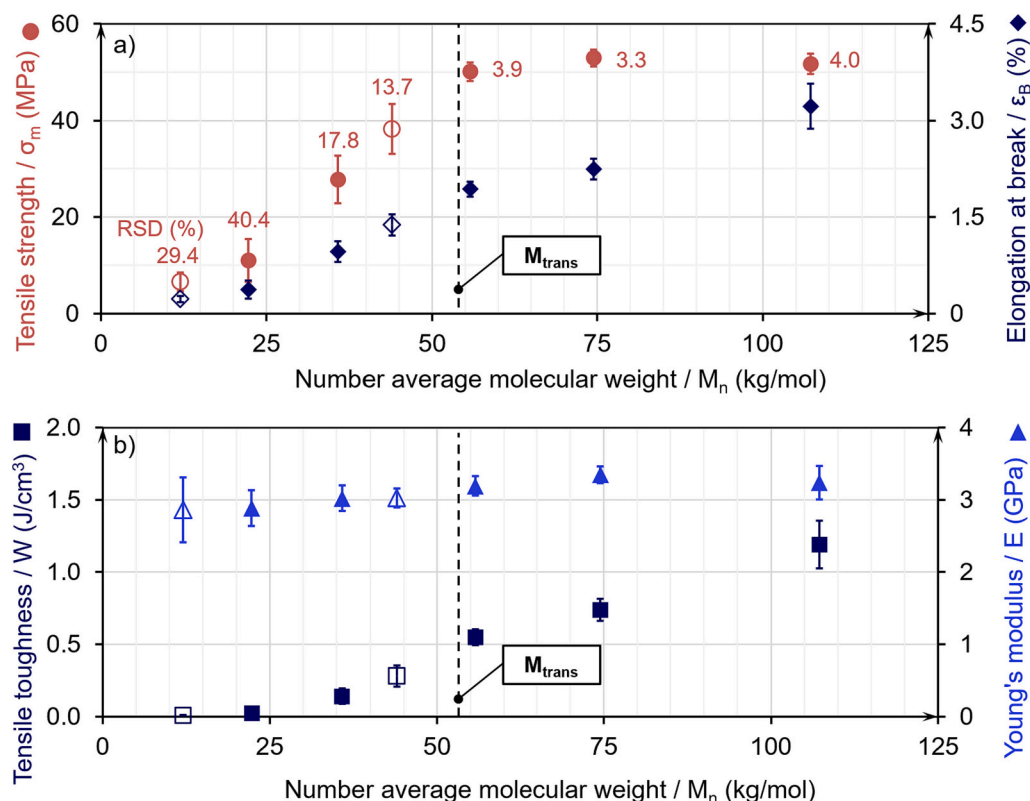**Fig. 13.** Changes in the shape of the tensile curve due to irradiation.

Fig. 14. Changes in tensile properties due to UV-C irradiation: a) tensile strength and elongation at break, b) tensile toughness and Young's modulus. The full markers are the properties associated with the measured molecular weights, the empty markers are the measured properties associated with the molecular weights estimated from linear regression. For the fitting, we used only the full marker data. RSD means relative standard deviation.

$$\sigma = \sigma_\infty - \frac{K_5}{M_n} \tag{7}$$

where K_5 (MPa·kg/mol) is the Flory constant and σ_∞ (MPa) is the limiting tensile strength for very high molecular weights (both are fitted parameters). The curve of tensile strength as a function of molecular weight generally follows two shapes: it monotonously increases without a plateau or is asymptotic until a given value [54,55]. Based on our results we can conclude that the Flory equation gives a good prediction only if there is an increase in strength. We also found that elongation at break and the tensile work can be good parameters to characterise degradation, since the relationship of both with M_n follows a trend. We applied the Flory equation to tensile strength, and linear equations to elongation at break and tensile work (Fig. 15). To make the predictions comparable, we normalised tensile properties with the corresponding

maximum values. The goodness of the fittings was characterised with the coefficient of determination (R^2) and the root mean squared error (*RMSE*). The *RMSE* and the R^2 values show that models based on elongation at break and tensile work give more accurate estimations than tensile strength. The model using tensile strength is less accurate above the transition molecular weight. Meanwhile, predictions based on elongation at break and tensile work describe the whole region well.

3.7.3. Molecular interpretation of the ductile-brittle transition

The transition between brittle and ductile behaviour means a change in the failure mechanism. Under tensile loading, glassy polymers can exhibit two dominant failure mechanisms: chain scission and chain pull-out [56]. Above M_{trans} failure occurs at a quasi-constant stress value with a small (approximately 4 %) relative standard deviation (*RSD*) (Fig. 14/a). The energy required to break covalent bonds is constant along the
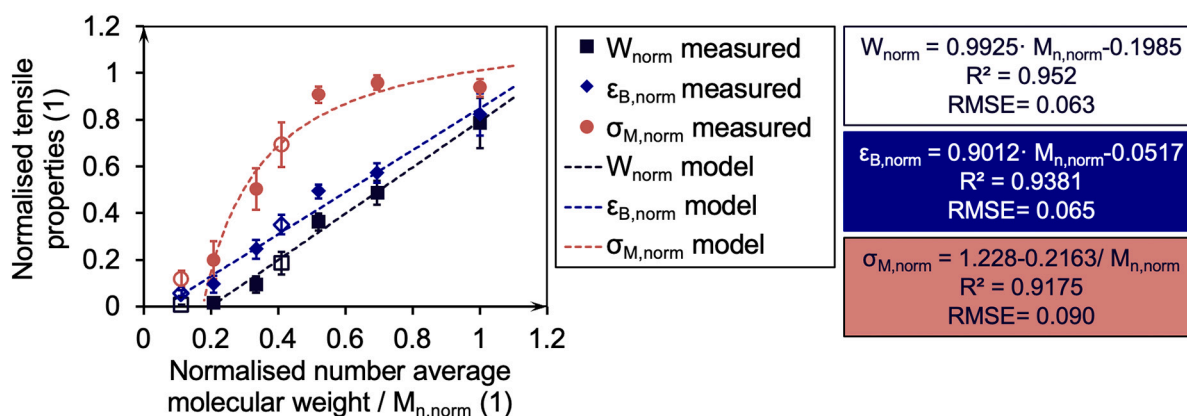
Fig. 15. The goodness of fitting for various models relating tensile properties to molecular weight.

molecular chain for the C—O and C—C bonds [57]. Therefore, it is more likely that the failure mechanism above M_{trans} is chain breakage. First, the secondary bonds break under loading, and the molecules start to slide past each other and align in the loading direction due to conformational changes. Secondary bonds can also re-form as the chains move and change their conformation, causing the elongation plateau in the tensile diagram. However, molecular entanglement acts as a spatial barrier that hinders and limits the motion of the molecules. In a system of longer entangled chains, the energy required to pull a chain from such a restriction may exceed the energy needed to break the covalent bond within the molecule, therefore in this case, primary bonds break. As irradiation time is increased, chains shorten and the number of chain ends increases, so the crack may develop sooner, thus the length of the elongation plateau is reduced. But the dominant failure mechanism

remains unchanged as long as yielding (after yield strength is reached) is observed (Fig. 16). Please note, that these considerations apply to the tensile speed used for the tests. At higher test speeds the failure mechanism may vary. Below the transition molecular weight, the dominant failure mode is chain pullout. The whole system is more prone to statistical errors and its more stochastic nature can also be observed in the increase of *RSD* (Fig. 14). Meanwhile, the energy required to break the primary bonds does not change, therefore the probability of a chain slipping is far higher than the probability of a chain breaking.

4. Conclusion

We investigated the material property changes of amorphous polylactic acid (PLA) films subjected to UV-C irradiation for up to 8 h. The
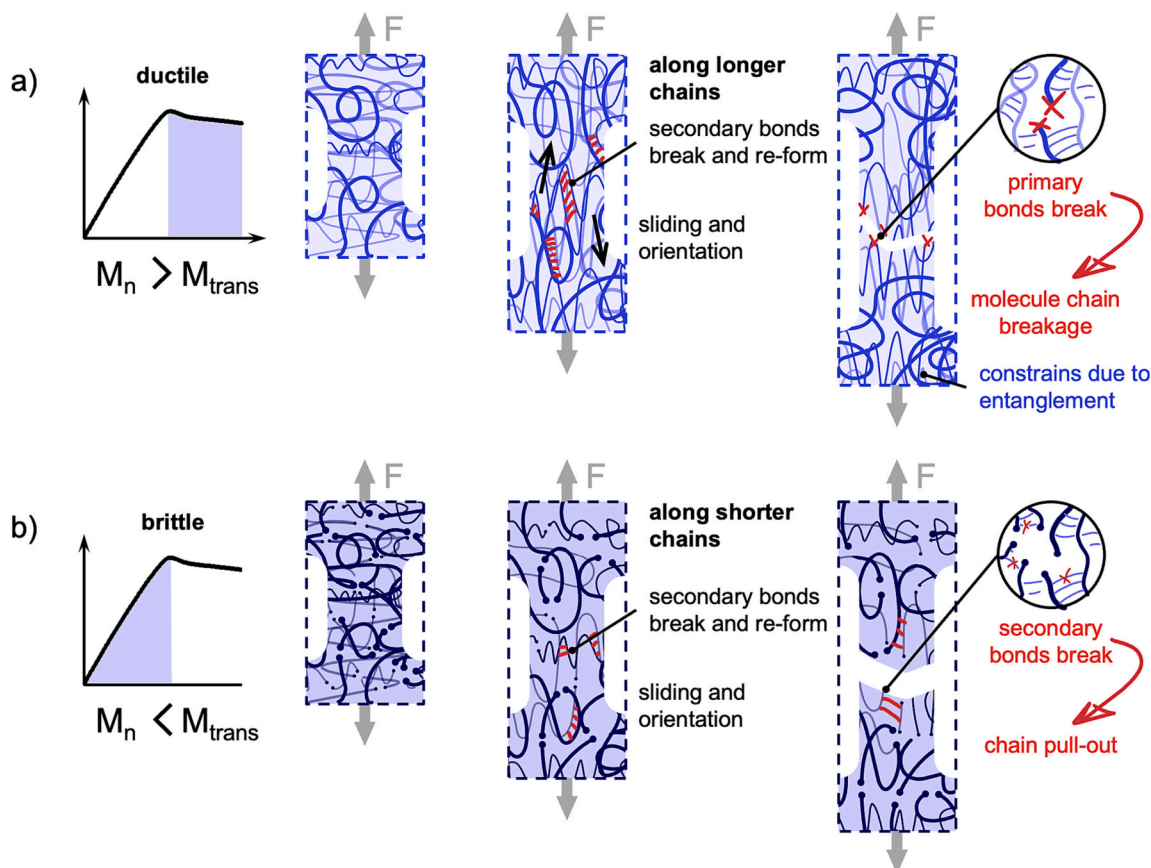

Fig. 16. Molecular interpretation of the ductile (a) and brittle (b) regions of the tensile curve.

samples were irradiated in a custom-built chamber equipped with two light sources of 254 nm wavelength commonly used for sterilisation. We found that the degradation mechanism is noncatalytic random scission and the number-average molecular weights (measured with GPC) decreased by 94 % in 8 h. Based on the changes in chemical structure identified with FTIR and UV–Vis, a possible photodegradation mechanism was proposed. Based on the tensile tests UV-C degradation does not affect the yield strength and the tensile modulus. A transition molecular weight (M_{trans}) can be defined above which only elongation decreases, and below which tensile strength decreases too. M_{trans} thus divides ductile and brittle material behaviour. We found that at the M_{trans} failure mode changes from chain breakage to chain pull-out. Dynamic rheological measurements showed that up to 0.5 h of irradiation, complex viscosity exhibited shear-thinning, then it shifted to nearly Newtonian and then showed shear-thickening characteristics. The elongation at break and the loss modulus curves, as well as the area under the tensile and Han curves, were suitable for characterising the level of degradation for more than 80 %. Our results show that this type of PLA film can withstand 13 cycles of UV-C sterilisation without significant changes in tensile strength and modulus. We measured the irradiance along the vertical distance and angle of incidence, based on which we drew a 3D irradiance map. These findings will contribute to the design of disinfection devices and can help in the proper sterilisation of medical equipment with different geometries.

CRediT authorship contribution statement

Ábris Dávid Virág: Conceptualization, Investigation, Methodology, Validation, Writing – original draft. **Csenge Tóth:** Conceptualization, Investigation, Writing – original draft, Visualization, Formal analysis. **Kolos Molnár:** Resources, Funding acquisition, Supervision, Writing – review & editing.

Declaration of competing interest

Data availability

Data will be made available on request.

Acknowledgements

Appendix A. Appendices

One-way ANOVA analyses of stress and modulus resulted in *p* values of $p = 0.016$ and $p < 0.001$, respectively. These p values were less than the chosen significance level ($\alpha = 0.05$), therefore we carried out post hoc tests (Tables A.1 and Table A.2.). Cases with the same letter in the Grouping column of the tables are considered statistically identical. The cases that do not share a letter are significantly different. The results show that the stress and modulus values of the examined degraded cases are identical to the initial, undegraded values.

Table A.1
Grouping information of stress values using the Tukey Method and 95 % confidence.

Irradiation time (h)	Number of measurements	Mean value of tensile stresses (MPa)	Grouping	
0	9	51.7	A	B
0.25	9	52.9	A	–
0.5	9	50.1	–	B

Table A.2
Grouping information of modulus values using the Games-Howell Method and 95 % Confidence.

Irradiation time (h)	Number of measurements	Mean value of moduli (GPa)	Grouping	
0	9	3.239	A	B
0.25	9	3.349	A	–
0.5	9	3.194	A	B
0.75	9	3.028	–	B
1	9	3.025	–	B
2	9	2.888	–	B
4	9	2.862	A	B

Appendix B. Supplementary data

Supplementary data to this article can be found online at https://doi.org/10.1016/j.ijbiomac.2023.126336.

References

[1] A. George, M.R. Sanjay, R. Srisuk, J. Parameswaranpillai, S. Siengchin, A comprehensive review on chemical properties and applications of biopolymers and their composites, Int. J. Biol. Macromol. 154 (2020) 329–338, https://doi.org/10.1016/j.ijbiomac.2020.03.120.

[2] S. Farah, D.G. Anderson, R. Langer, Physical and mechanical properties of PLA, and their functions in widespread applications — a comprehensive review, Adv. Drug Deliv. Rev. 107 (2016) 367–392, https://doi.org/10.1016/j.addr.2016.06.012.

[3] C.S. Wu, D.Y. Wu, S.S. Wang, Heat-regulating polylactic acid/silica aerogel composite fabric: Peparation and characterisation, Express Polym Lett 16 (2022) 21–33, https://doi.org/10.3144/expresspolymlett.2022.3.

[4] A. Costa, T. Encarnação, R. Tavares, T. Todo Bom, A. Mateus, Bioplastics: innovation for Green transition, Polymers (Basel). 15 (2023), https://doi.org/10.3390/polym15030517.

[5] F. Lopresti, L. Botta, V. La Carrubba, G. Attinasi, L. Settanni, G. Garofalo, R. Gaglio, Physical and antibacterial properties of PLA electrospun mats loaded with carvacrol and nisin, Express Polym Lett 16 (2022) 1083–1098, https://doi.org/10.3144/expresspolymlett.2022.79.

[6] N.F. Zaaba, M. Jaafar, A review on degradation mechanisms of polylactic acid: hydrolytic, photodegradative, microbial, and enzymatic degradation, Polym. Eng. Sci. 60 (2020) 2061–2075, https://doi.org/10.1002/pen.25511.

[7] F.D. Kopinke, M. Remmler, K. Mackenzie, M. Möder, O. Wachsen, Thermal decomposition of biodegradable polyesters—II. Poly(lactic acid), Polym. Degrad. Stab. 53 (1996) 329–342, https://doi.org/10.1016/0141-3910(96)00102-4.

[8] M.A. Elsawy, K.H. Kim, J.W. Park, A. Deep, Hydrolytic degradation of polylactic acid (PLA) and its composites, Renew. Sust. Energ. Rev. 79 (2017) 1346–1352, https://doi.org/10.1016/J.RSER.2017.05.143.

[9] E. Ikada, Photo- and bio-degradable polyesters. Photodegradation behaviors of aliphatic polyesters, J. Photopolym. Sci. Technol. 10 (1997) 265–270, https://doi.org/10.2494/photopolymer.10.265.

[10] E. Olewnik-Kruszkowska, I. Koter, J. Skopińska-Wiśniewska, J. Richert, Degradation of polylactide composites under UV irradiation at 254 nm, J. Photochem. Photobiol. A Chem. 311 (2015) 144–153, https://doi.org/10.1016/j.jphotochem.2015.06.029.

[11] S. Therias, J.-F. Larché, P.-O. Bussière, J.-L. Gardette, M. Murariu, P. Dubois, Photochemical behavior of Polylactide/ZnO nanocomposite films, Biomacromolecules. 13 (2012) 3283–3291, https://doi.org/10.1021/bm301071w.

[12] K. Janczak, G.B. Dąbrowska, A. Raszkowska-Kaczor, D. Kaczor, K. Hrynkiewicz, A. Richert, Biodegradation of the plastics PLA and PET in cultivated soil with the participation of microorganisms and plants, Int. Biodeterior. Biodegradation 155 (2020), https://doi.org/10.1016/j.ibiod.2020.105087.

[13] W. Sikorska, M. Musioł, B. Nowak, J. Pajak, S. Labuzek, M. Kowalczuk, G. Adamus, Degradability of polylactide and its blend with poly[(R,S)-3-hydroxybutyrate] in industrial composting and compost extract, Int. Biodeterior. Biodegradation 101 (2015) 32–41, https://doi.org/10.1016/j.ibiod.2015.03.021.

[14] Y. Kara, K. Molnár, Decomposition behavior of stereocomplex PLA melt-blown fine fiber mats in water and in compost, J. Polym. Environ. (2022) https://doi.org/10.1007/s10924-022-02694-w.

[15] S. Agustin-Salazar, N. Gamez-Meza, L.À. Medina-Juàrez, H. Soto-Valdez, P. Cerruti, From nutraceutics to materials: effect of resveratrol on the stability of polylactide, ACS Sustain. Chem. Eng. 2 (2014) 1534–1542, https://doi.org/10.1021/sc5002337.

[16] S. Pérez Davila, L. González Rodríguez, S. Chiussi, J. Serra, P. González, How to sterilise polylactic acid based medical devices? Polymers (Basel). 13 (2021) https://doi.org/10.3390/polym13132115.

[17] M. Biasin, A. Bianco, G. Pareschi, A. Cavalleri, C. Cavatorta, C. Fenizia, P. Galli, L. Lessio, M. Lualdi, E. Tombetti, A. Ambrosi, E.M.A. Redaelli, I. Saulle, D. Trabattoni, A. Zanutta, M. Clerici, UV-C irradiation is highly effective in inactivating SARS-CoV-2 replication, Sci. Rep. 11 (2021), https://doi.org/10.1038/s41598-021-85425-w.

[18] M. Buonanno, B. Ponnaiya, D. Welch, M. Stanislauskas, G. Randers-Pehrson, L. Smilenov, F.D. Lowy, D.M. Owens, D.J. Brenner, Germicidal efficacy and mammalian skin safety of 222-nm UV light, Radiat. Res. 187 (2017) 483–491, https://doi.org/10.1667/RR0010CC.1.

[19] R. Resti-Costa, C. von Z. Negrão, J.F. Shimizu, A. Nagai, R.S.N. Tavares, D. Adamoski, W. Costa, M.A. Fontoura, T.J. da Silva, A. de Barros, A. Girasole, M. de Carvalho, V. de C. Teixeira, A.L.B. Ambrosio, F. Granja, J.L. Proença-Módena, R.E. Marques, S.M.G. Dias, UV 254 nm is more efficient than UV 222 nm in inactivating SARS-CoV-2 present in human saliva, Photodiagn. Photodyn. Ther. 39 (2022), https://doi.org/10.1016/j.pdpdt.2022.103015.

[20] G. Volchenkov, Experience with UV-C air disinfection in some Russian hospitals†, Photochem. Photobiol. 97 (2021) 549–551, https://doi.org/10.1111/php.13418.

[21] M.S. Islam, A. Patras, B. Pokharel, Y. Wu, M.J. Vergne, L. Shade, H. Xiao, M. Sasges, UV-C irradiation as an alternative disinfection technique: study of its effect on polyphenols and antioxidant activity of apple juice, Innov. Food Sci. Emerg. Technol. 34 (2016) 344–351, https://doi.org/10.1016/j.ifset.2016.02.009.

[22] B.M. Andersen, H. Bånrud, E. Bøe, O. Bjordal, F. Drangsholt, Comparison of UV C light and Chemicals for Disinfection of surfaces in hospital isolation units, Infect. Control Hosp. Epidemiol. 27 (2006) 729–734, https://doi.org/10.1086/503643.

[23] N. Ribeiro, G.C. Soares, V. Santos-Rosales, A. Concheiro, C. Alvarez-Lorenzo, C. A. García-González, A.L. Oliveira, A new era for sterilisation based on supercritical CO2 technology, J Biomed Mater Res B Appl Biomater 108 (2020) 399–428, https://doi.org/10.1002/jbm.b.34398.

[24] T. Standau, C. Zhao, S.M. Castellón, C. Bonten, V. Altstädt, Chemical modification and foam processing of polylactide (PLA), Polymers (Basel). 11 (2019), https://doi.org/10.3390/polym11020306.

[25] M. Musioł, W. Sikorska, G. Adamus, H. Janeczek, J. Richert, R. Malinowski, G. Jiang, M. Kowalczuk, Forensic engineering of advanced polymeric materials. Part III - Biodegradation of thermoformed rigid PLA packaging under industrial composting conditions, Waste Management. 52 (2016) 69–76, https://doi.org/10.1016/J.WASMAN.2016.04.016.

[26] C.P. Sabino, F.P. Sellera, D.F. Sales-Medina, R.R.G. Machado, E.L. Durigon, L. H. Freitas-Junior, M.S. Ribeiro, UV-C (254nm) lethal doses for SARS-CoV-2, Photodiagn. Photodyn. Ther. 32 (2020), 101995, https://doi.org/10.1016/j.pdpdt.2020.101995.

[27] D. Mills, D.A. Harnish, C. Lawrence, M. Sandoval-Powers, B.K. Heimbuch, Ultraviolet germicidal irradiation of influenza-contaminated N95 filtering facepiece respirators, Am. J. Infect. Control 46 (2018) e49–e55, https://doi.org/10.1016/j.ajic.2018.02.018.

[28] S. Narla, A.B. Lyons, I. Kohli, A.E. Torres, A. Parks-Miller, D.M. Ozog, I. H. Hamzavi, H.W. Lim, The importance of the minimum dosage necessary for UVC decontamination of N95 respirators during the COVID-19 pandemic, Photodermatol Photoimmunol Photomed. 36 (2020) 324–325, https://doi.org/10.1111/phpp.12562.

[29] N. Yasuda, Y. Wang, T. Tsukegi, Y. Shirai, H. Nishida, Quantitative evaluation of photodegradation and racemisation of poly(l-lactic acid) under UV-C irradiation, Polym. Degrad. Stab. 95 (2010) 1238–1243, https://doi.org/10.1016/j.polymdegradstab.2010.03.034.

[30] A. Gleadall, J. Pan, M.A. Kruft, M. Kellomäki, Degradation mechanisms of bioresorbable polyesters. Part 1. Effects of random scission, end scission and autocatalysis, Acta Biomater. 10 (2014) 2223–2232, https://doi.org/10.1016/j.actbio.2013.12.039.

[31] L. Santonja-Blasco, A. Ribes-Greus, R.G. Alamo, Comparative thermal, biological and photodegradation kinetics of polylactide and effect on crystallisation rates, Polym. Degrad. Stab. 98 (2013) 771–784, https://doi.org/10.1016/j.polymdegradstab.2012.12.012.

[32] T. Suzuki, K. Takahashi, H. Uehara, T. Yamanobe, Application and analysis of a DSC-Raman spectroscopy for indium and poly(lactic acid), J. Therm. Anal. Calorim. 113 (2013) 1543–1549, https://doi.org/10.1007/s10973-013-3098-z.

[33] G. Kister, G. Cassanas, M. Vert, Effects of morphology, conformation and configuration on the IR and Raman spectra of various poly(lactic acid)s, Polymer (Guildf). 39 (1998) 267–273, https://doi.org/10.1016/S0032-3861(97)00229-2.

[34] C. Zhang, C. Man, W. Wang, L. Jiang, Y. Dan, Degradation of poly(L-lactide) films under ultraviolet irradiation and water bath, Polym Plast Technol Eng 50 (2011) 810–817, https://doi.org/10.1080/03602559.2011.551970.

[35] C. Man, C. Zhang, Y. Liu, W. Wang, W. Ren, L. Jiang, F. Reisdorffer, T.P. Nguyen, Y. Dan, Poly (lactic acid)/titanium dioxide composites: preparation and performance under ultraviolet irradiation, Polym. Degrad. Stab. 97 (2012) 856–862, https://doi.org/10.1016/J.POLYMDEGRADSTAB.2012.03.039.

[36] E. Zuza, J.M. Ugartemendia, A. Lopez, E. Meaurio, A. Lejardi, J.R. Sarasua, Glass transition behaviour and dynamic fragility in polylactides containing mobile and rigid amorphous fractions, Polymer (Guildf). 49 (2008) 4427–4432, https://doi.org/10.1016/j.polymer.2008.08.012.

[37] T.G. Fox, P.J. Flory, Second-order transition temperatures and related properties of polystyrene. I. Influence of molecular weight, J. Appl. Phys. 21 (1950) 581–591, https://doi.org/10.1063/1.1699711.

[38] P.J. Flory, Thermodynamics of crystallisation in high polymers. IV. A theory of crystalline states and fusion in polymers, copolymers, and their mixtures with diluents, J. Chem. Phys. 17 (1949) 223–240, https://doi.org/10.1063/1.1747230.

[39] T.G. Fox, S. Loshaek, Influence of molecular weight and degree of crosslinking on the specific volume and glass temperature of polymers, J. Polym. Sci. 15 (1955) 371–390, https://doi.org/10.1002/pol.1955.120158006.

[40] M.C. Righetti, Amorphous fractions of poly(lactic acid), in: R. Di Lorenzo Maria Laura, Androsch (Eds.), Synthesis, Structure and Properties of Poly(Lactic Acid), Springer International Publishing, Cham, 2018, pp. 195–234, https://doi.org/10.1007/12_2016_14.

[41] W.P. Cox, E.H. Merz, Correlation of dynamic and steady flow viscosities, J. Polym. Sci. 28 (1958) 619–622, https://doi.org/10.1002/pol.1958.1202811812.

[42] M. Przybysz-Romatowska, J. Haponiuk, K. Formela, Poly(ε-caprolactone)/poly (lactic acid) blends compatibilised by peroxide initiators: comparison of two strategies, Polymers (Basel). 12 (2020), https://doi.org/10.3390/polym12010228.

[43] A.A. Marek, V. Verney, Influence of the viscoelastic regime onto the UV reactivity of poly(lactic acid), Eur. Polym. J. 110 (2019) 138–144, https://doi.org/10.1016/j.eurpolymj.2018.11.016.

[44] T.G. Fox, S. Loshaek, Isothermal viscosity-molecular weight dependence for long polymer chains, J. Appl. Phys. 26 (1955) 1080–1082, https://doi.org/10.1063/1.1722154.

[45] J.M. Dealy, D.J. Read, R.G. Larson, 5 - linear viscoelasticity—Behavior of molten polymers, in: J.M. Dealy, D.J. Read, R.G. Larson (Eds.), Structure and Rheology of Molten Polymers (Second Edition), Hanser, 2018, pp. 147–195, https://doi.org/10.3139/9781569906125.005.

[46] J.R. Dorgan, J. Janzen, M.P. Clayton, S.B. Hait, D.M. Knauss, Melt rheology of variable L -content poly(lactic acid), J Rheol (N Y N Y). 49 (2005) 607–619, https://doi.org/10.1122/1.1896957.

[47] J.R. Dorgan, J.S. Williams, D.N. Lewis, Melt rheology of poly(lactic acid): entanglement and chain architecture effects, J Rheol (N Y N Y). 43 (1999) 1141–1155, https://doi.org/10.1122/1.551041.

[48] P. Szatkowski, L. Czechowski, J. Gralewski, M. Szatkowska, Mechanical properties of polylactide admixed with carbon nanotubes or graphene nanopowder, Materials. 14 (2021), https://doi.org/10.3390/ma14205955.

[49] B. Pinpathomrat, C. Narita, A. Yokoyama, K. Yamada, Evaluation of degradation of ultraviolet-C irradiated polylactic acid/carbon-fiber composites using fluorescence spectroscopy, Adv. Compos. Mater. 31 (2022) 195–207, https://doi.org/10.1080/09243046.2021.1943108.

[50] Z. Bin Ahmad, M.F. Ashby, Failure-mechanism maps for engineering polymers, J. Mater. Sci. 23 (1988) 2037–2050, https://doi.org/10.1007/BF01115766.

[51] J. Pabiot, J. Verdu, The change in mechanical behavior of linear polymers during photochemical aging, Polym. Eng. Sci. 21 (1981) 32–38, https://doi.org/10.1002/pen.760210106.

[52] B. Fayolle, L. Audouin, J. Verdu, Oxidation induced embrittlement in polypropylene — a tensile testing study, Polym. Degrad. Stab. 70 (2000) 333–340, https://doi.org/10.1016/S0141-3910(00)00108-7.

[53] P.J. Flory, Tensile strength in relation to molecular weight of high polymers, J. Am. Chem. Soc. 67 (1945) 2048–2050, https://doi.org/10.1021/ja01227a506.

[54] A.R. Cooper, Mechanical properties of polymers: the influence of molecular weight and molecular weight distribution, Journal of Macromolecular Science, Part C. 8 (1972) 57–199, https://doi.org/10.1080/15321797208068169.

[55] R.W. Nunes, J.R. Martin, J.F. Johnson, Influence of molecular weight and molecular weight distribution on mechanical properties of polymers, Polym. Eng. Sci. 22 (1982) 205–228, https://doi.org/10.1002/pen.760220402.

[56] P. Prentice, Influence of molecular weight on the fracture of poly(methyl methacrylate) (PMMA), Polymer (Guildf). 24 (1983) 344–350, https://doi.org/10.1016/0032-3861(83)90275-6.

[57] C.-A. Dai, E.J. Kramer, J. Washiyama, C.-Y. Hui, Fracture toughness of polymer Interface reinforced with Diblock copolymer: effect of Homopolymer molecular weight, Macromolecules. 29 (1996) 7536–7543, https://doi.org/10.1021/ma960533l.